Continental Shelf Research 112 (2016) 68–77

Contents lists available at ScienceDirect

Continental Shelf Research

journal homepage: www.elsevier.com/locate/csr

Research papers

Temporal variation in water intrusion of a tidal frontal system and distribution of chlorophyll in the Seto Inland Sea, Japan

Tomohiro Komorita *, Xinyu Guo, Naoki Yoshie, Naoki Fujii [1], Hidetaka Takeoka

Center for Marine Environmental Studies, Ehime University, 2-5 Bunkyo-Cho, Matsuyama 790-8577, Japan

ARTICLE INFO

Article history:
Received 20 January 2015
Received in revised form
14 October 2015
Accepted 23 October 2015
Available online 30 October 2015

Keywords:
Tidal front
Nutrient cycles
Thermal stratification
Phytoplankton
Coastal zone
Seto Inland Sea

ABSTRACT

Monthly field surveys conducted from April to November 2009 in a tidal front in the Seto Inland Sea, Japan provided a spatial and temporal dataset for investigating seasonal variations in nutrient supply and the formation of a chlorophyll *a* (Chl-*a*) maximum. The upward diffusive flux of nutrients is estimated from observational data but it accounted for less than 5% of the nutrients needed to support the primary production of phytoplankton in the front area of the stratification region when the density difference between the surface layer and bottom layer is greater than 0.5 kg m^{-3}. Instead of vertical diffusion, the lateral intrusion of water with high nutrient concentration from the mixed area represented the major nutrient supply in the front area. The depth of the lateral intrusion changed with the month: the surface layer in July became the middle layer in August. According to the calculation of numerical model, an anti-clockwise circulation is intensified by removing river runoff (i.e., low precipitation) in this study area, and the change of lateral intrusion is likely caused by the change of anti-clockwise circulation along with the temporal variation in river runoff. Consequently, the Chl-*a* peak appeared in the vicinity of the surface front (up to 3 μg L^{-1}) in July, but was in the subsurface (up to 9 μg L^{-1}) in August. Diatom species were a relatively minor taxa of the phytoplankton community up to July, although a relatively high $Si(OH)_4$-Si concentration (up to 20 μmol L^{-1}) was confirmed. In contrast, the subsurface Chl-*a* maximum (SCM) in August was mainly comprised of diatoms as evidenced by the reduction of both $Si(OH)_4$-Si and Si/N from the surface to subsurface layer (0–20 m depth). Therefore, the supply of both nutrients and the seed population necessary for the formation of the SCM results from the tidal frontal system and phytoplankton assemblages within the tidal front system should be varied on a monthly basis.

1. Introduction

Tidal fronts develop seasonally in many coastal waters (Simpson and Hunter, 1974), forming a transition zone between stratified regions developed as a result of solar heating and regions of weak tidal currents and mixed regions due to strong tidal currents. Traditionally, the stratified region has been considered to be a two-layered system in which the transfer of nutrients from the bottom layer to the surface layer is suppressed by strong thermal stratification, allowing phytoplankton to remain in the euphotic layer for extended periods of time causing the development of nutrient depletion. In the mixed region, phytoplankton remain in the euphotic layer for only a short period of time due to strong vertical mixing and growth is likely to be limited by light availability; consequently, depletion of inorganic nutrients does not occur. Optimal nutrient and light conditions are therefore achieved only in the frontal zone between the mixed and stratified regions (Le Fevre, 1986; Mann, 2000). As a result, an area of high chlorophyll concentration forms in the surface layer or in the subsurface layer of the frontal zone (Franks and Chen, 1996; Holligan, n.d.; Martínez and Ortega, 2007; O'Boyle and Silke, 2009).

Several researchers have proposed an alternate model to the two-layered system. In the proposed three-layered system of the stratified region at the tidal front, stratification is separated into surface, bottom, and middle layers, and nutrients from the bottom layer of the stratified region are carried to the subsurface layer through the adjacent mixed region by newly described mechanisms such as “nutrient bypass” (Takeoka et al., 1993), “tidally-fed pump” (Pedersen, 1994), and “tidal pumping” (Richardson et al., 2000). In such three-layered systems, a subsurface chlorophyll maximum (SCM) may develop in response to the horizontal

* Corresponding author. *Present address*: Faculty of Environmental and Symbiotic Sciences, Prefectural University of Kumamoto, 3-1-100, Tsukide, Kumamoto 862-8502, Japan.
E-mail address: komorita@pu-kumamoto.ac.jp (T. Komorita).
[1] Present address: Institute of Lowland and Marine Research, Saga University, 1, Honjyo-Cho, Saga 840-8502, Japan.

http://dx.doi.org/10.1016/j.csr.2015.10.015
0278-4343/

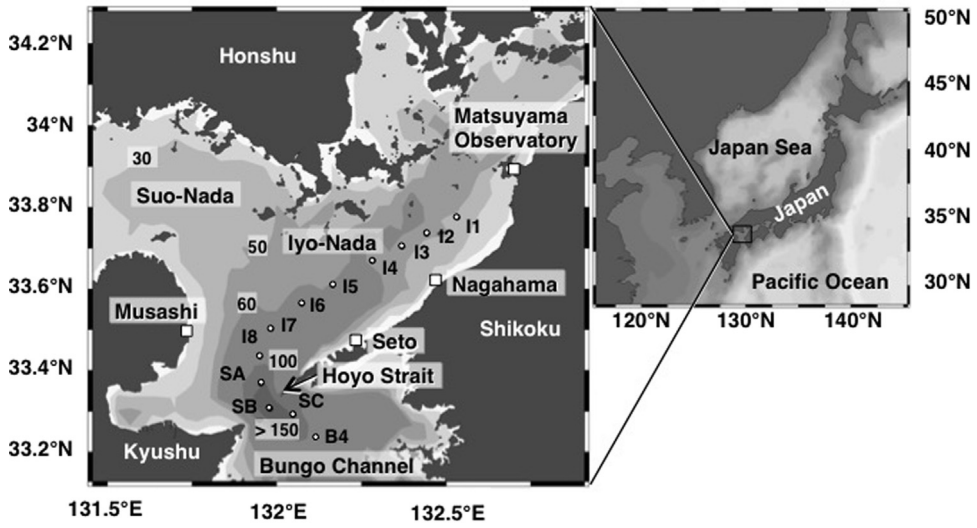

Fig. 1. Study area and sampling station locations. On the left panel, the open circles represent sampling stations and the numbers in the white boxes represent water depth in meters.

intrusion of nutrient-rich water into the photic zone (Richardson et al., 2000) and the introduction of a seed population of phytoplankton species by the horizontal intrusion from the mixed region (Kaas et al., 1991; Lund-Hansen and Vang, 2004; Nielsen et al., 1990).

Tidal fronts are generated in early spring and disappear in early autumn mainly because of seasonal variations in sea surface heat flux, wind forcing, and river discharge (Yanagi and Tamaru, 1990). However, most observations of tidal fronts are carried out only in the summer when the tidal front is fully developed (Gowen and Bloomfield, 1996; Holligan, n.d.; Townsend and Thomas, 2002). By making observations only on established tidal fronts, seasonal variations in biogeochemical dynamics and biogeochemical cycles related to the tidal fronts remain largely unknown.

The Seto Inland Sea is a large, shallow, semi-enclosed sea in western Japan with an area of 17,000 km^2 and mean water depth of 37 m (Fig. 1). This area has high biological productivity with annual primary production of 218 g C m^{-2} yr^{-1} in the water column (Tada et al., 1998). The annual fish catch in the sea is 3.2–28 times larger than that in other typical semi-enclosed seas such as the Chesapeake Bay, the Baltic Sea, the North Sea, and the Mediterranean Sea (Takeoka, 2002). The deep but narrow straits in the Seto Inland Sea produce strong tidal currents, leading to thorough vertical mixing of the water column in the straits, which remain mixed throughout the year (Takeoka, 2002). In contrast, the wide and shallow areas between the straits, known as *nada* in Japanese, have weak tidal currents and strong stratification develops in the summer. Consequently, several tidal fronts form between the *nadas* and straits (Takeoka, 2002). The strait-*nada* system, which is a tidal front system, along with the efficient transport of nutrients from the bottom layer of the *nada* (=stratified region) to the euphotic layer near tidal fronts is considered to be one of the most important mechanisms for sustaining the high biological productivity in the Seto Inland Sea.

In the eastern part of the Seto Inland Sea, tidal fronts develop in spring and are sustained until early autumn (Yanagi and Koike, 1987) between the Hoyo Strait and the Iyo-*Nada* (Fig. 1). In summer, intrusion of water carrying nutrients from the Hoyo Strait into the middle layer of Iyo-*Nada* (Takeoka et al., 1993) is suggested to stimulate the photosynthetic activity of phytoplankton assemblages (Yamamoto et al., 2000). In the central part of Iyo-*Nada* (i.e., stratified region), residual currents show an anticlockwise circulation from spring to summer (Chang et al., 2009). The anti-clockwise circulation should be affected by several meteorological forcings such as solar heating, river discharge (i.e., rainfall), and wind forcing (Yu et al., in press). Thus, it is easily expected that the biogeochemical cycle related to the middle layer intrusion also varied with those seasonal meteorological forcings. However, field studies to examine seasonal variation in phytoplankton and nutrient distributions near the front have not been documented.

In this study, we conducted monthly field surveys from April to November 2009 to span the development and disruption of stratification in the Seto Inland Sea. We investigated spatio-temporal variation in physical (water stratification), chemical (nutrient), and biological (phytoplankton assemblages) processes. We used the vertical distribution patterns of water temperature, salinity, density, dissolved inorganic nutrients [NO_3+NO_2-N and $Si(OH)_4$-Si], and chlorophyll *a* (Chl-*a*) (both total and size-fractionated) in the tidal front system to examine the formation and disruption of the stratified region. Based on field data, we evaluated the horizontal intrusion of mixed region water into the middle layer of the stratified region, and we demonstrate the seasonal variation of horizontal intrusion, dominant phytoplankton taxa and nutrient composition in the tidal front system. Finally, we discuss the time series variation of the phytoplankton assemblages within a tidal frontal system based on the examination of the relationship between the Chl-*a* peak and the depth of the horizontal intrusion and the supply of seed species to the phytoplankton community.

2. Materials and methods

Ten field surveys were conducted from April to November 2009 (Table 1) in the three regions of Iyo-*Nada* with eight stations (Stns. I1–I8: approximately 50–80 m in depth), Hoyo Strait with three stations (Stns. SA–SC: over 150 m in depth) and Bungo Channel with one station (Stn. B4: approximately 80 m in depth) (Fig. 1). The daily tidal range recorded at the Matsuyama Observatory (Fig. 1) was obtained for survey days. The M_2 constituent was dominant over the entire Seto Inland Sea, and the amplitude of the M_2 tidal current constituent reached approximately 1.5 m s^{-1} in the Hoyo Strait (Takeoka, 2002).

At each station, a rosette sampling unit equipped with conductivity, temperature and depth probes, a chlorophyll fluorometer (JFE Advantech Co., Ltd.), and ten 3 l Niskin bottles (JFE

Table 1
Cruise information. Tidal difference (cm), and station and depth of size fraction Chl-*a* collection on each sampling occasion.

Dates in 2009	Tidal range (cm)	Size fraction of Chl-*a*	
		Stn.	Depth
23-Apr	278	I5, I8, B4	0, 10, 20, 30, 50 m
3-Jun[a]	271	I5, I8, B4	0, 10, 20, 30, 50 m
25-Jun	361	I4	20, 25, 30, 50 m
		I8, B4	0, 10, 20, 30, 50 m
22-Jul	385	I4, I8, B4	0, 10, 20, 30, 50 m
23-Aug	300	I4, I8, B4	0, 10, 20, 30, 50, 60 m
29-Aug	149	I5, I8, B4	0, 10, 20, 25, 30, 50 m
17-Sep	330	I4, I8	0, 10, 20, 30, 50 m
1-Oct	239	I4, I8, B4	0, 10, 20, 30, 50 m
14-Oct	248	I4, I8, B4	0, 10, 20, 30, 50 m
20-Nov	273	I4	0, 15, 30, 50, 60 m
		I8, B4	0, 20, 40, 60, 80 m

[a] Stns. SB and SC were observed on 5 June 2009.

Advantech Co., Ltd.) was deployed for sampling from the sea surface to 1 m above the sea bottom. Water sampling for nutrients [NO_3+NO_2-N and $Si(OH)_4$-Si] was conducted at 10 m intervals at all stations. In addition, water sampling for total and size-fractionated Chl-*a* was conducted from 5 to 20 m interval at Stns. I4 or I5, and I8 and B4 (Table 1).

After collection, samples for nutrient analysis were immediately filtered through disposable filter units (25CS DISMIC 0.45 μm, Advantec), and the filtrate was stored at −40 °C until analysis on a Bran+Luebbe Auto Analyzer III using the method of Strickland and Parsons (1972).

For Chl-*a* analysis, water samples (300 ml) were filtered through a cascaded 3 stage filter holder system (Sartorius) under low vacuum (< 100 mm Hg) with filters of three pore sizes (10, 2 and 0.2 μm, Whatman Nuclepore membrane filter). The filters were soaked in 5.0 ml DMF (N, N-dimethylformamide) and frozen in a deep freezer (−40 °C) until analysis. The Chl-*a* concentration in the extract was measured with a fluorometer (TD-700, Turner Designs) using the method of Welschmeyer (1994). The results of total Chl-*a* concentration were used to construct a calibration curve for converting measured in vivo fluorescence from the CTD cast values by the fluorometer to Chl-*a* concentration (r^2 ranged between 0.595 and 0.918, varying for different cruises).

Daily mean temperature and precipitation from April to November were obtained at three meteorological stations (Nagahama, Seto, and Musashi; see Fig. 1 for locations). The 10 min average wind velocity data collected at the meteorological station of Seto were obtained for the periods of 19–22 July and 19–22 August, which were both 3 days prior to our survey cruises.

3. Calculation

Water in the middle layer of a three-layered stratified region formed by mixing water from the two (i.e., surface and bottom waters) or three (i.e., surface, bottom, and mixed area water) zones is represented by straight and curved lines, respectively, in a temperature–salinity (*T*–*S*) diagram (Takeoka et al., 1993) (Fig. 2a). Based on this concept, the deviation of data from two-end member mixing line on the *T*–*S* diagram reflects the presence of water from other regions in the middle layer of stratified region (Fig. 2a). To quantify the contribution of water from regions other than the surface and bottom layers, we plotted the temperature and salinity of the simple mixing line, a straight line from the surface water (surface end member: mean from depth of 5 m to the surface) to the bottom water (bottom end member: mean from depth of 5 m

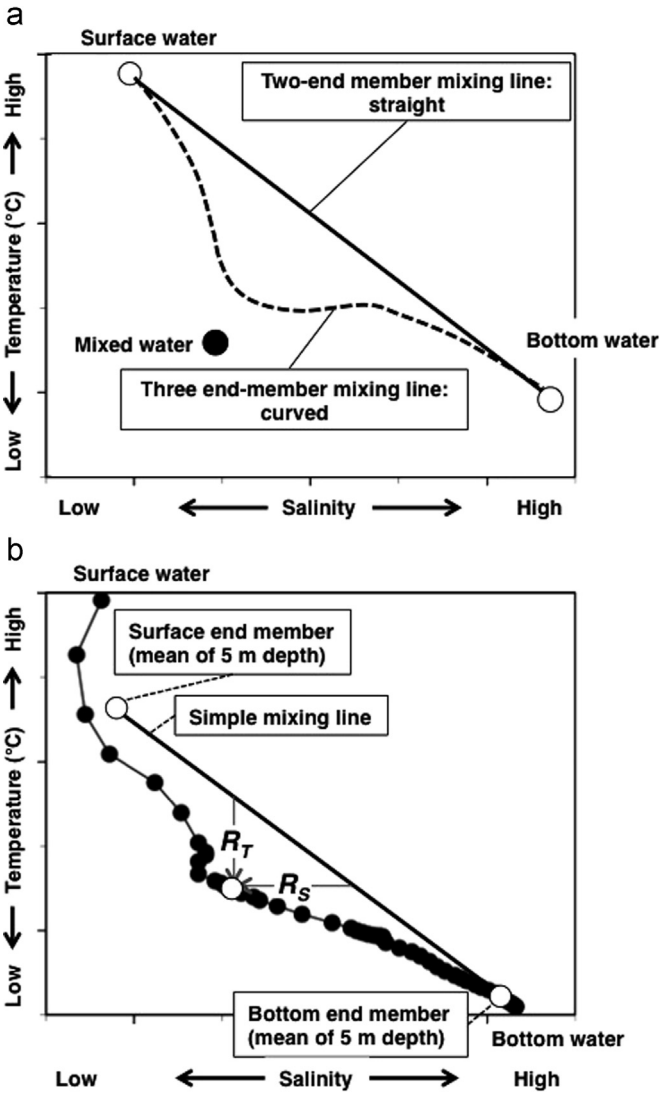

Fig. 2. (a) Schematic diagram of the two and three end-member mixing models, and (b) temperature–salinity (*T*–*S*) diagram showing the schematic for estimating intrusion strength (R_T and R_S).

above the bottom to the bottom) along with the actual data, and then calculated the temperature and salinity difference between the actual data and the simple mixing line, R_T and R_S, *respectively*, at each depth and at each station (Fig. 2b). The formula for *R* is

$$R_{Td} = T_d - (a^* S_d + b), \quad (1)$$

$$R_{Sd} = S_d - (T_d - b)/a, \quad (2)$$

where subscript *d* is depth, *S* is salinity measured at depth *d*, *T* is water temperature at depth *d*.

A positive R_T and R_S indicate an intrusion of comparatively warmer and saline water, respectively, while a negative R_T and R_S indicate an intrusion of comparatively colder and less saline water, respectively.

4. Results

4.1. Meteorological data

The tidal range was between 239 and 385 cm, except for 29 August (Table 1). Mean daily air temperature and precipitation

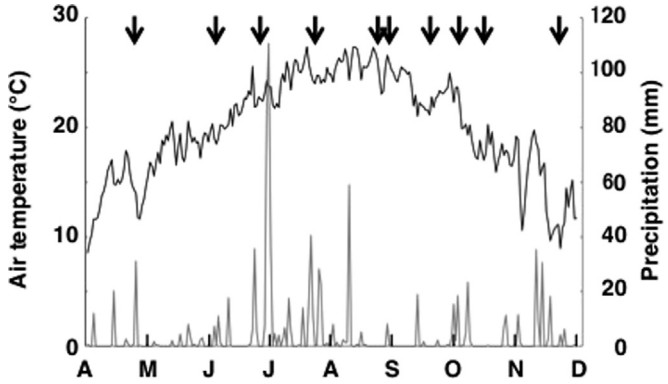

Fig. 3. Seasonal variation in air temperature and precipitation. Arrows indicate sampling surveys.

data collected at three meteorological stations (Nagahama, Seto, and Musashi meteorological stations) were used to assess seasonal variation of air temperature and precipitation in our sampling region (Fig. 3). The air temperature increased from 15.8 °C in April to 24.3 °C in July, and was within the range of 21.8–27.4 °C during the summer (June–August) and decreased gradually starting in September. Daily precipitation was 110 mm on 30 June, and the mean daily precipitation was higher from June to July (7.0 mm) than in August (2.8 mm).

4.2. Seasonal variation

Fig. 4a shows an isopleth depicting the time series of the density difference between the surface (2 m depth) and bottom (deepest available data) layers. We defined the stratified period as having a density difference greater than 0.5 kg m^{-3}. Using this criterion, the stratified region was shown to extend from approximately 40 km (Stns. I3–I6) to approximately 80 km (Stns. I1–SA) in distance during the period from 3 June to 29 August. Density differences were mainly attributable to water temperature (Fig. 4b), but salinity played a contributing role in July (Fig. 4c). According to Fig. 4, stratification was strengthening from June to July and weakening from July to August.

Fig. 5(a) and (b) shows the isopleth at a depth of 20 m (between surface and bottom layer) of residual R_T and R_S as defined by Eq. (1), respectively. The R_T showed a larger range during period of stratification (ca. −1 to 2 °C) than after the stratified period (less than 0.5 °C). Over the entire season, the R_T was positive, indicating the intrusion of relatively warm water from May to July, indicating the intrusion of relatively cold water from July to August. The R_S was positive on July and slightly negative on August in the central part of Iyo-*Nada*, indicating the intrusion of relatively saline and less saline water, respectively (Fig. 5b).

The temporal variation in physical and biogeochemical variables at the center of the stratified region (Stns. I4 and I5) is shown in Fig. 6. In the surface water, the temperature reached 26.3 °C in late August (Fig. 6a), and the salinity dropped to 32.8 in July (Fig. 6b) due to high precipitation (Fig. 3). Although salinity was the lowest in the surface water in July, water from the subsurface to the bottom (depths of approximately 10–60 m) showed the lowest salinity in August (Fig. 6b). Chl-*a* concentration showed a peak of 2.4 μg L^{-1} in the subsurface layer (approximately 20–30 m in depth) before July but reached a higher value after August (approx. 4 μg L^{-1} at a depth of 24 m on 29 August; Fig. 6d). A large fraction (> 10 μm) Chl-*a* ranged between 0.07 and 0.34 in the surface layer (depth of 0–20 m) from April to June and increased over 0.5 after August (Fig. 6e). NO_3+NO_2-N concentration was below 1 μmol L^{-1} in the surface layer (depth of 0–20 m) from April to October. A clear nitracline could be identified in the

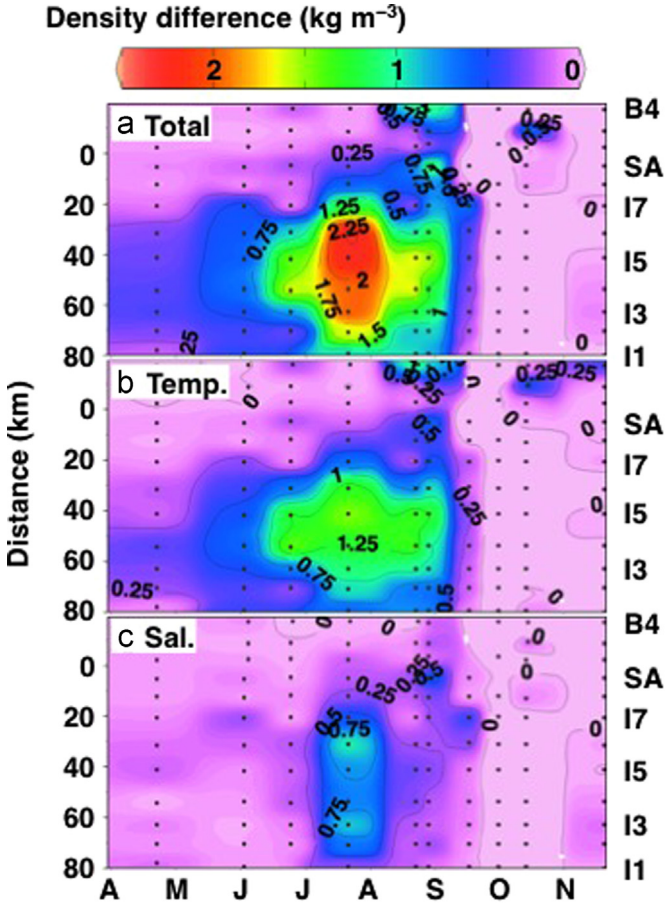

Fig. 4. Seasonal variation for differences in density between the surface layer at a depth of 2 m and bottom water at all sampling stations based on (a) sigma-*t*, (b) temperature, and (c) salinity. Distance is from Hoyo Strait at station SB along the sampling transect.

middle layer between depths of 20–30 m during the period of stratification. $Si(OH)_4$-Si concentration was relatively high (above 10 μmol L^{-1}) in the surface layer before July and decreased to approximately 1.0 μmol L^{-1} after August. Since the reduction of $Si(OH)_4$-Si concentration after August coincided with the increase in overall Chl-*a* concentration and large-size fraction Chl-*a* (Fig. 6d and e), the dominant phytoplankton taxa likely changed from non-diatom species before July to diatom species after August.

4.3. Difference between pre-July and post-August

As shown in Fig. 6, the physical and biogeochemical variables in the center of the stratified region showed a dramatic change between the July and August surveys. Here, we make a comprehensive analysis of the possible differences in the physical environment.

To analyze the existence of differences in the pattern of winds between July and August, wind rose diagrams were made based on 10 min average wind velocity and wind direction at the meteorological observatory of Seto (Fig. 1) during the 3 days preceding each sampling survey (Fig. 7). There was little difference in the wind fields. The prevailing winds in both July and August were a relatively strong southerly winds (8–12 m s^{-1}) that accounted for a small ratio (< 5.0%) of the winds experienced in the area in these 2 months. Therefore, it is difficult to expect that winds caused the differences in the data for the two months presented in Fig. 6.

Mean precipitation at the three meteorological stations exceeded 10 mm per day in the 6 days during the last two weeks of July, and reached 40.5 mm per day before the sampling day of 21

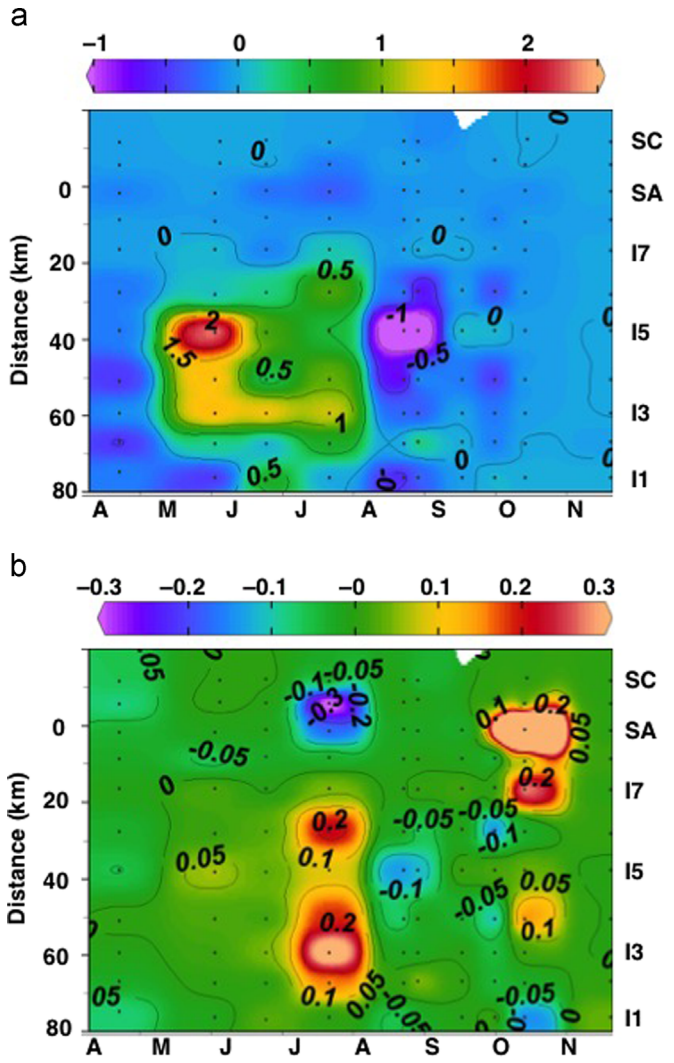

Fig. 5. Seasonal variation in the residuals from the simple mixing line at subsurface layer (depth of 20 m) based on (a) temperature (R_T) and (b) salinity (R_S).

July (Fig. 8a). The vertical distribution of water temperature (Fig. 8b) showed the presence of a cold water mass in the bottom layer of the stratified region (Stns. I4–I6). The lowest sigma-*t* (21.7) was found in the surface layer of the stratified region (Fig. 8d) where low salinity (Fig. 8c) was found along with high water temperature (Fig. 8b). R_T and R_S indicating deviation from the simple mixing line increased to above 1 °C and 0.2, respectively, around the subsurface layer (depth of 10–20 m) of the stratified region (Stns. I2–I6). The *T*–*S* diagram for the center of the stratified region (Stn. I5) shows a gentle curve to the mixed region (Stn. SC) and partially overlaps with data for the frontal region (Stns. I7 and SA) (Fig. 8g). Chl-*a* concentration was high (up to 3 $\mu g\ L^{-1}$) in the surface layer (approximate depth of 10 m) of the frontal region (Stns. I7–SA) where a large horizontal gradient of water temperature and salinity exists (Fig. 8b and c).

In August, there was little rainfall (0.2–8.2 mm per day) (Fig. 9a). The survey conducted on 22 August suggests that thermal stratification was still in place in the stratified region (Stns. I3–I6) (Fig. 9b). However, the salinity gradient from the surface layer to the bottom layer showed a difference of less than 0.4 and was smaller than the gradient observed in July. Salinity in the surface layer was higher in August than in July but that in the bottom layer was lower in August than in July (Fig. 9c). The difference in density between the surface layer and bottom layer was also smaller in August than in July (Fig. 9d). The R_T and R_S in August were negative and showed low values in the subsurface layer (depth approximately 10–20 m) of the stratified region (Stn. I5) (Fig. 9e, f). Chl-*a* concentration was higher in the subsurface layer at Stns. I1 and I5 (Fig. 9g) where the residual is relatively high (Fig. 9e). The *T*–*S* plot of subsurface layer (approx. 10–20 m) on the stratified region (i.e., Stn. I5) curves in the opposite direction as that in the mixed and frontal regions (i.e., both temperature and salinity were lower than that of mixed water) (Fig. 9h). Thus, the opposite curve indicates that the intrusion of water has less saline and low water temperature.

4.4. Nutrient upward flux on the stratified region in August

The highest Chl-*a* concentration was observed in the subsurface layer in the stratified region in August (Fig. 9g). To determine whether the vertical flux of nutrients could sustain the SCM, we calculated the vertical nitrogen diffusive flux across the nitracline using the following equation,

$$\text{Nitrogen flux } \left(\text{mmol m}^{-2}\ \text{d}^{-1}\right) = -K_Z(\Delta N/\Delta Z), \quad (3)$$

where K_Z ($\text{m}^2\ \text{d}^{-1}$) is the vertical eddy diffusion coefficient, ΔN is the difference in nitrogen concentration (mmol m^{-3}) above and below the nitracline, and ΔZ is the nitracline thickness. Taking ΔN as the difference between the mean NO_3+NO_2-N concentration in the surface layer and the middle layer in the central area of the stratified region on 22 August (Fig. 6f), ΔZ value of 20 m, or the distance between the center of surface layer (10 m depth) and the depth of 30 m (Fig. 6), and using the K_Z value of Takeoka et al. (1986) (0.9–3.5 $\text{m}^2\ \text{d}^{-1}$) that was the same order as at the top of bottom cold water in this study area was calculated by the 3D numerical model (Yu et al., in press), the diffusive flux for NO_3+NO_2-N became 0.1–0.4 mmol N $\text{m}^{-2}\ \text{d}^{-1}$.

5. Discussion

Typical nutrient sources driving the Chl-*a* peak in frontal regions are suggested as (1) horizontal intrusion from the mixed region in the surface layer (Holligan et al., 1984), (2) horizontal intrusion from the mixed region in the middle layer (Lund-Hansen and Vang, 2004; Pedersen, 1994; Takeoka et al., 1993), and (3) vertical upward flux from the bottom layer to the surface layer (Lips et al., 2011; Lund-Hansen, 2011). In the case of horizontal intrusion in the surface layer, the peak Chl-*a* concentration is generally found in the vicinity of the surface front; in the case of horizontal intrusion in the subsurface layer, the peak Chl-*a* concentration is in the subsurface layer of a stratified region (Le Fevre, 1986). In this study, the peak Chl-*a* concentration was in the vicinity of the front in July (Fig. 8f), but the peak was in the subsurface in August (Fig. 9f). Thus, the nutrient source driving the surface Chl-*a* peak in July was probably surface intrusion while that for the subsurface Chl-*a* peak in August was subsurface intrusion.

Previous field studies suggest that under certain conditions, upward nutrient diffusive flux is one of the important nutrient sources for the development of the SCM (Lund-Hansen, 2011). The primary production in our study area was found to be approximately 700 mg C $\text{m}^{-2}\ \text{d}^{-1}$ in July and September (Tada et al., 1998), and the nitrogen-based production of phytoplankton was estimated to be approximately 9 mmol N $\text{m}^{-2}\ \text{d}^{-1}$, assuming C/N=6.6 (Redfield et al., 1963). Since the upward diffusive flux of NO_3+NO_2-N (0.1–0.4 mmol N $\text{m}^{-2}\ \text{d}^{-1}$, Section 4.4) was less than 5% of the nutrients required to support the primary production of phytoplankton, it must represent a minor contribution to the available nutrient pool. Therefore, the middle layer intrusion of

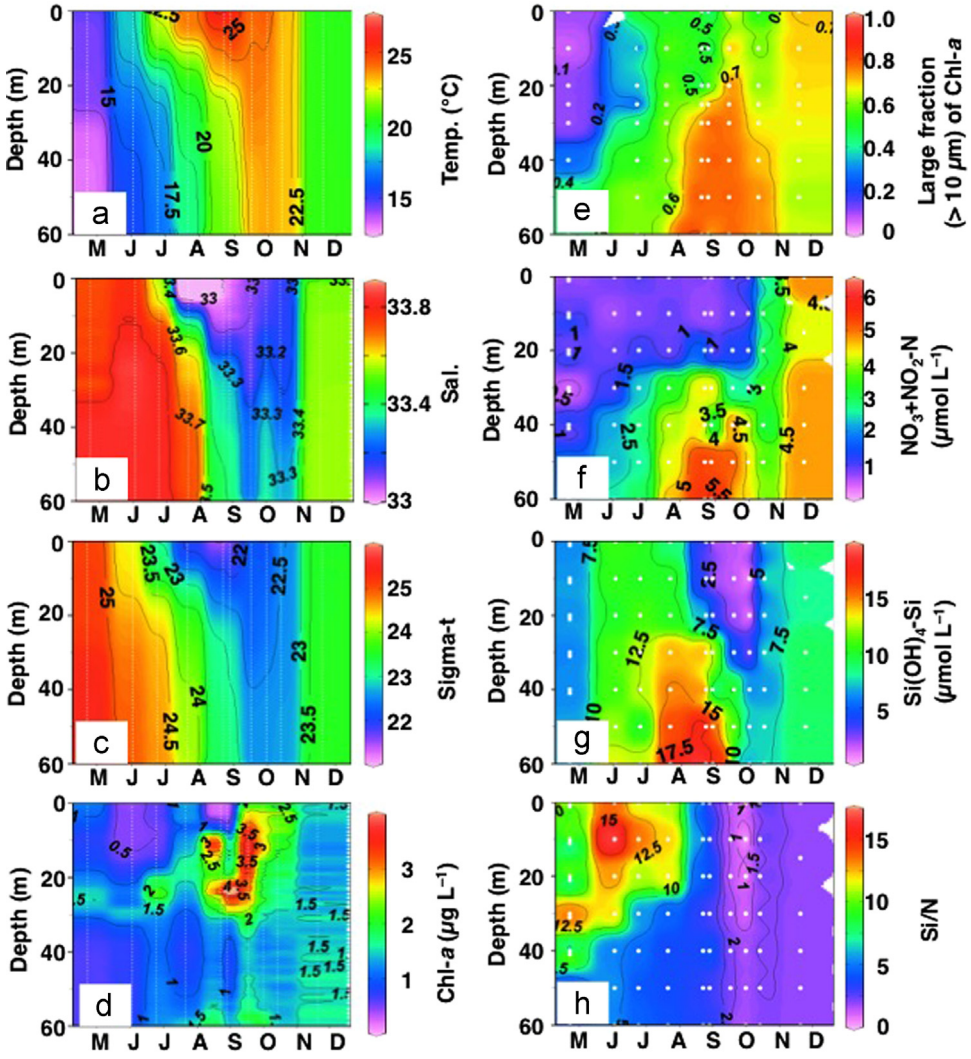

Fig. 6. Seasonal variation in vertical distribution of (a) temperature, (b) salinity, (c) sigma-t, (d) Chl-*a*, (e) large fraction of Chl-*a*, (f) NO_3+NO_2-N concentration, (g) $Si(OH)_4$-Si concentration, and (h) Si/N recorded at Stns. I4 and I5. All the data are the average of data from two stations (Stns. I4 and I5), except for large Chl-*a* fraction which was measured at only one station (Table 1).

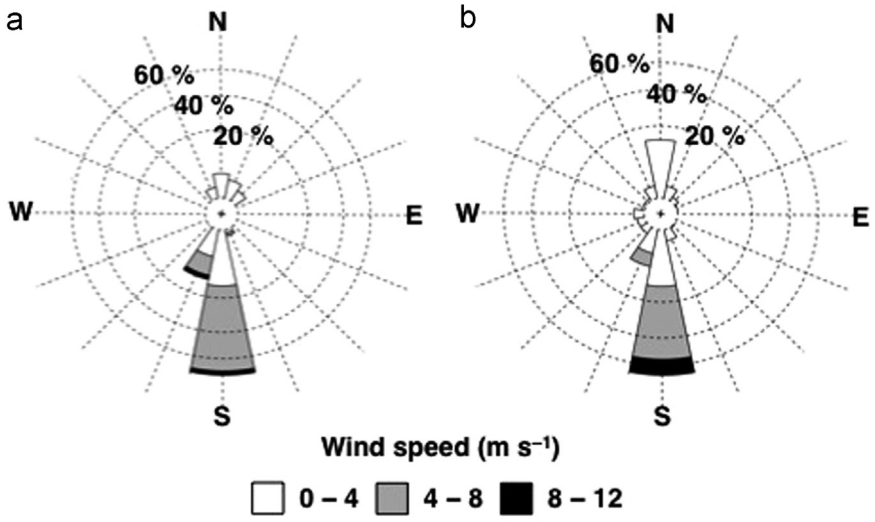

Fig. 7. 96-h Wind rose diagrams for the periods of (a) 19–22 July and (b) 19–22 August.

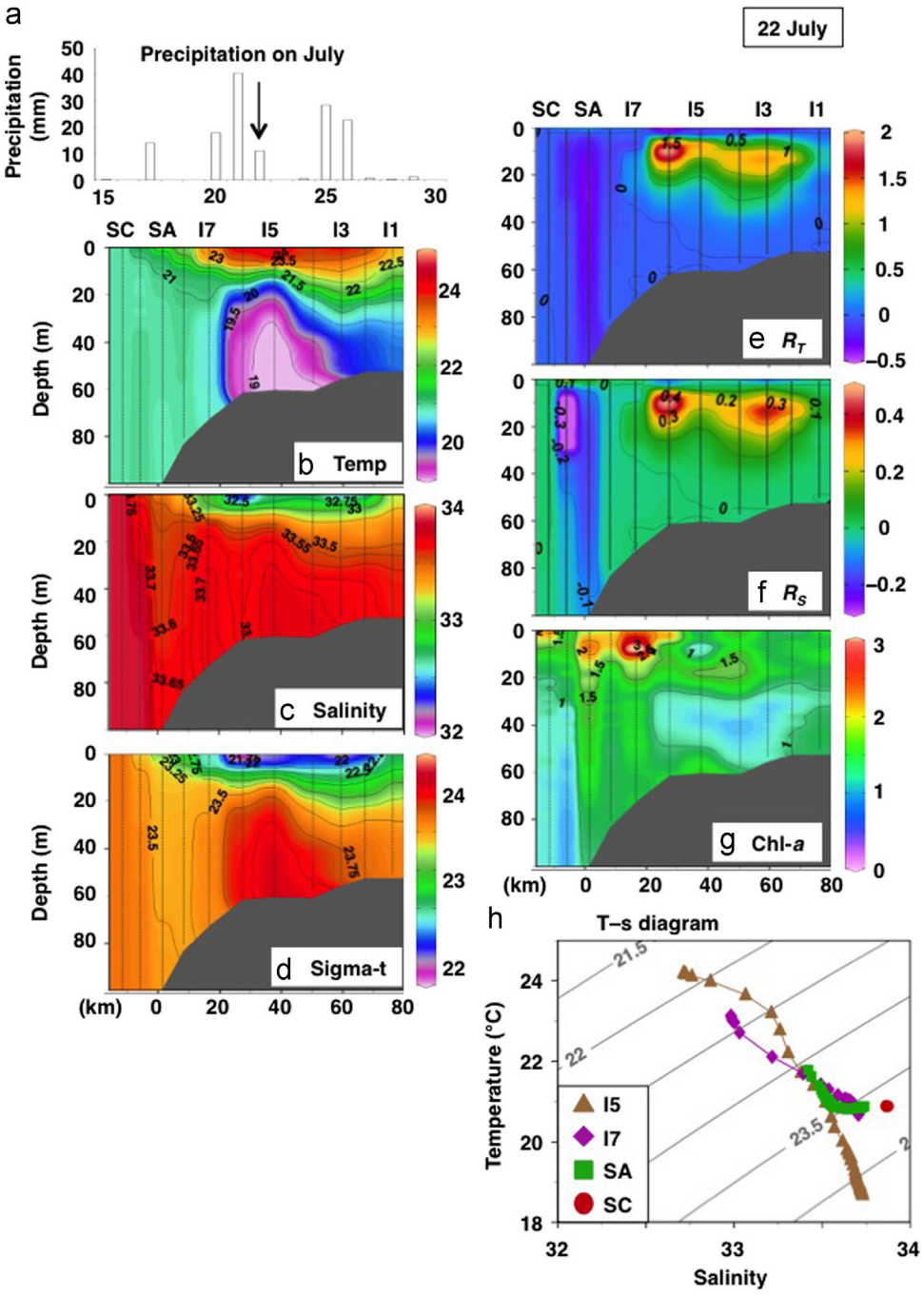

Fig. 8. (a) Precipitation in the vicinity of the 22 July sampling day and vertical distribution of (b) temperature, (c) salinity, (d) sigma-*t*, (e) residuals of temperature (R_T), (f) residuals of salinity (R_S), (g) Chl-*a* concentration, and (h) *T*–*S* diagram.

water from the mixed layer naturally becomes the most likely candidate for supplying nutrients to the SCM that was observed in August.

The horizontal intrusion of the mixed region water to the middle layer of the stratified region brings not only nutrients but also other materials, including seed populations of diatoms. As shown in Fig. 6, diatom species had a relatively minor representation among the taxa of the phytoplankton community before July, although $Si(OH)_4$-Si was relatively abundant. Only in August did diatom species become a major taxa in the phytoplankton community, and this shift was corroborated by the reduction of $Si(OH)_4$-Si (and Si/N) (Fig. 6g, h). Without a seed population of diatom species, this shift would not have been possible. Therefore, supply of a seed population of diatoms through the middle layer intrusion presumably occurred sometime in July and caused the subsequent uptake of dissolved inorganic nutrients, especially $Si(OH)_4$-Si. A similar case has been reported for the haptophycean flagellate *Chrysochromulina polylepis* which produces a subsurface bloom that is sustained by a middle layer intrusion of nutrients and seed populations from neighboring regions (Kaas et al., 1991).

According to a three-dimensional numerical ocean model for the Seto Inland Sea (Chang et al., 2009), anti-clockwise circulation in the summer is reproduced at the central part of Iyo-*Nada*, which is the stratified region in this study (Stns. I3–I6). The numerical modeling using high resolution Princeton Ocean Model (POM) for the Iyo-*Nada* (Yu et al., in press) shows that the anti-clockwise circulation is weakened by the addition of river discharges, which

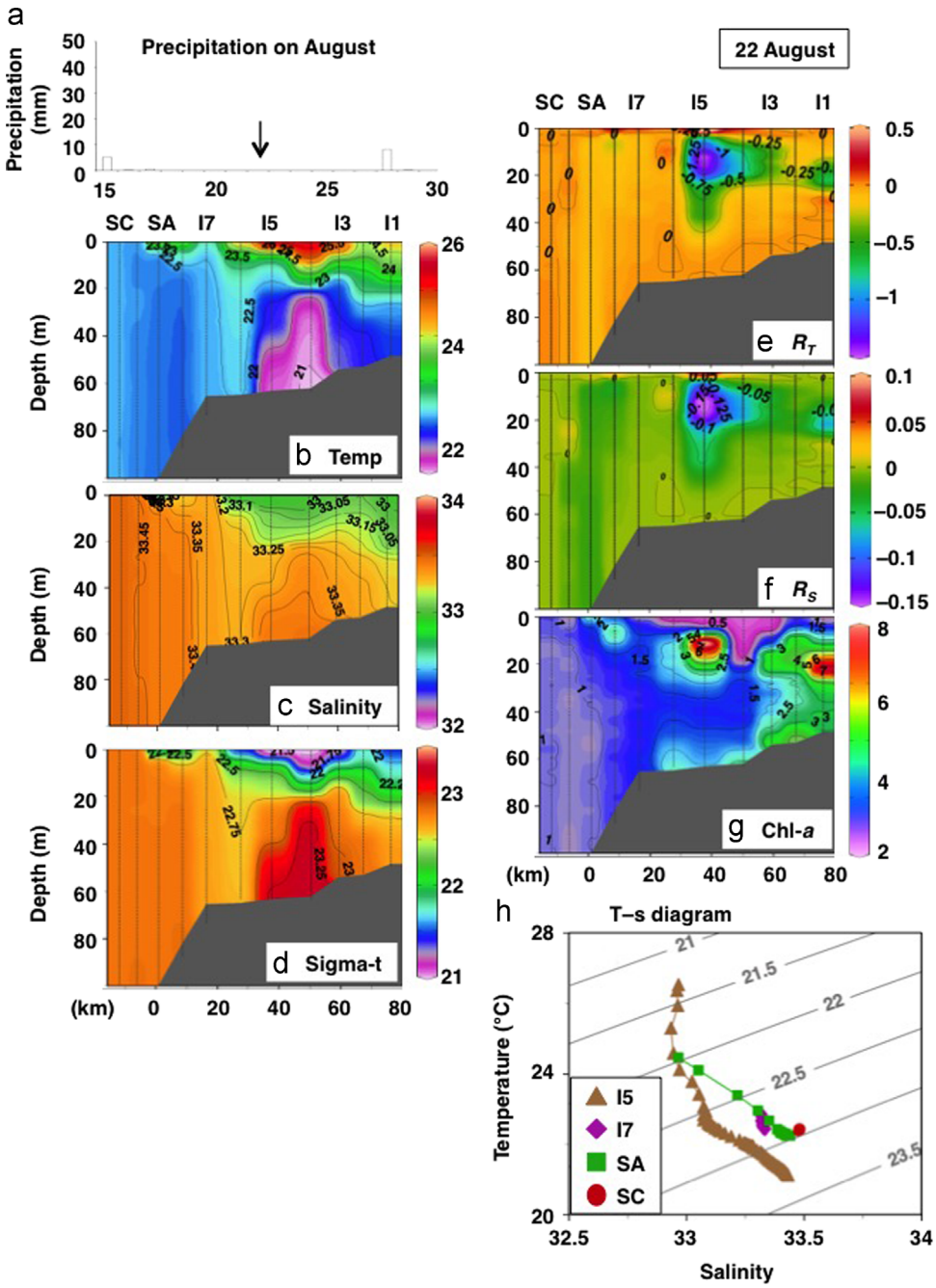

Fig. 9. (a) Precipitation in the vicinity of the 22 August sampling day and vertical distribution of (b) temperature, (c) salinity, (d) sigma-t, (e) residuals of temperature (R_T), (f) residuals of salinity (R_S), (g) Chl-*a* concentration, and (h) *T*–*S* diagram.

is related to the precipitation (Fig. 10). A direct interpretation of this result to our observation is that the anti-clockwise circulation was intensified between the July and August surveys due to the lower precipitation in August than in July (Figs. 3, 8a and 9a). With the intensification of anti-clockwise circulation, cold and less saline water originating from other regions around the sampling area could be introduced to the stratified region.

The differences of residual currents field between the case with river runoff (Fig. 10b) and the case without river runoff (Fig. 10a) do highlight the importance of intrusion from north-western part of Iyo-*Nada* (i.e., Suo-*Nada*, see Fig. 1 for its place) (Fig. 10c). The surface and bottom water of Suo-*Nada* are relatively less saline and colder, respectively, than the water in the middle layer of Iyo-*Nada* (Kobayashi et al., 2006). The anti-clockwise eddy across the Iyo-Nada and Suo-Nada should carry the cool and less saline Suo-Nada water to the study area. Moreover, 12 planktonic diatom species are detected in the surface sediment (including species have a resting stage such as *Thalassiosira* sp., *Coscinodiscus* sp., *Chaetoceros* sp., and so on) of Suo-*Nada* during summer (Sarker et al., 2009). Thus, it is likely that neighboring region (i.e., Suo-*Nada*) is one of the important sources of the cold and less saline water with seed population of diatom species.

6. Conclusion

Seasonal variation in the supply of nutrients in addition to an infusion of a seed population of diatoms in a tidal frontal system was examined based on the results of water mass structure, and nutrient and Chl-*a* distributions.

The source water of the middle layer intrusion to the stratified

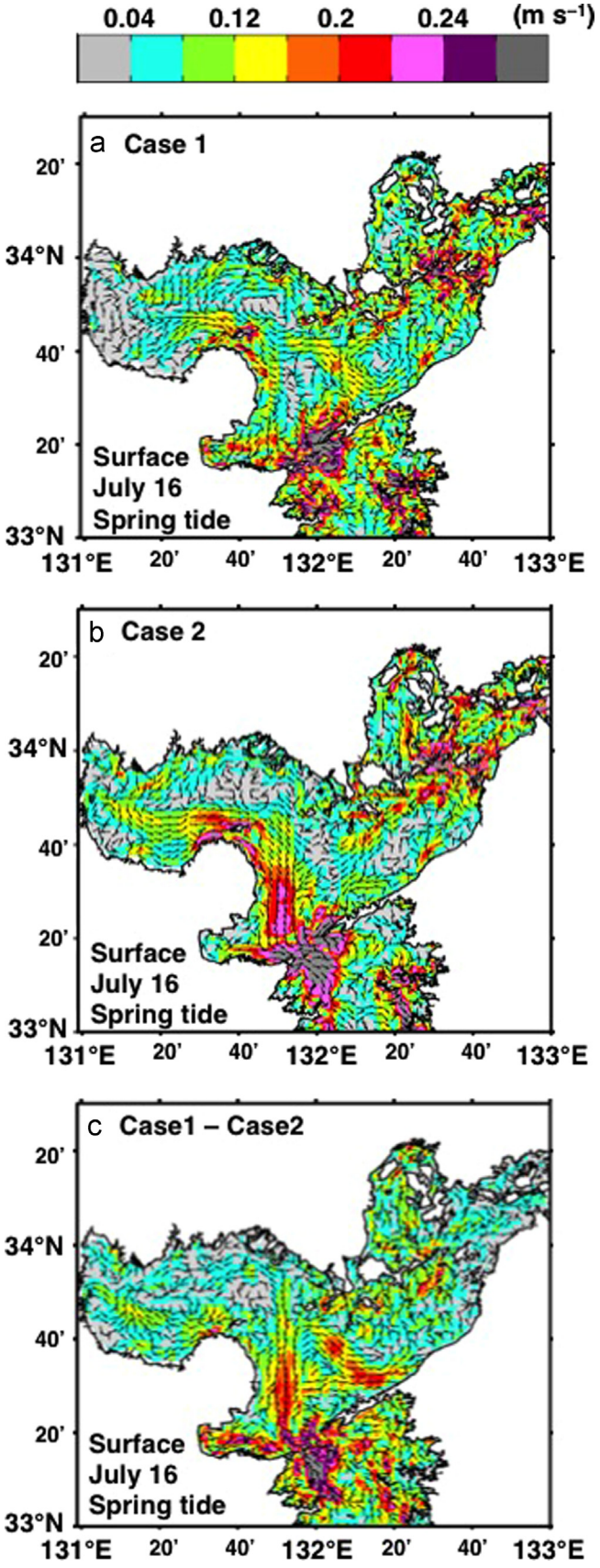

Fig. 10. Current at surface layer during spring tide calculated for (a) Case 1 (no river flow), (b) Case 2 (add River flow), and (c) Case 1 minus Case 2 (based on Yu et al., in press). The arrow shows the current direction and the color shows the current speed (m s^{-1}).

region changed from warm water to cold water. Such a drastic change was likely caused by an increase (decrease) of freshwater that weakens (strengthens) the anti-clockwise circulation in July (August) in the stratified region of Iyo-*Nada*. Moreover, formation of the SCM with diatoms requires not only a sufficiently high supply of nutrients but also the introduction of a seed population. Thus, phytoplankton assemblages within the tidal front system should be varied on a monthly basis.

To further clarify both the supply process of nutrients and the source of the seed population in other similar systems, possible sources and supply processes should be predicted by the numerical ocean model and verified by the field observations of phytoplankton composition. Moreover, bottle incubation experiments are also required, that is conducted by mixing possible source water of seed population and bottom water of stratified region (as nutrient source) under the medium light irradiance to reproduce the phytoplankton assemblages in the SCM.

Acknowledgment

We thank the captain of R/V *Isana*, Hidejiro Oonishi and Dr. Morrow J. Stewart for his critical reading of the English text. We also thank financial support from the JSPS KAKENHI (21310012) and a special project funded by Ehime University. The sampling surveys were conducted with the cooperation of members of the Center for Marine Environmental Studies.

References

Chang, P.H., Guo, X., Takeoka, H., 2009. A numerical study of the seasonal circulation in the Seto Inland Sea, Japan. J. Ocean. 65, 721–736.

Franks, P.J.S., Chen, C., 1996. Plankton production in tidal fronts: a model of Georges Bank in summer. J. Mar. Res. 54, 631–651.

Gowen, R., Bloomfield, S., 1996. Chlorophyll standing crop and phytoplankton production in the western Irish Sea during 1992 and 1993. J. Plankton Res. 18, 1735–1751.

Holligan, P., Williams, P.J.B., Purdie, D., Harris, R., 1984. Photosynthesis, respiration and nitrogen supply of plankton populations in stratified, frontal and tidally mixed shelf waters. Mar. Ecol. Prog. Ser. 17, 201–213.

Holligan, P.M., 1981. Biological Implications of Fronts on the Northwest European Continental Shelf. Philos. Trans. R. Soc. A Math. Phys. Eng. Sci. 302, 547–562.

Kobayashi, S., Fujiwara, T., Tada, M., Tsukamoto, H., Toyoda, T., 2006. The distributions of nitrogen (N), phosphorus (P), silicon (Si) and nutrient ratios during the stratified season in the Seto Inland Sea. Oceanogr. Jpn. 15, 283–297 (in Japanese with English abstract).

Le Fevre, J., 1986. Aspects of the biology of frontal systems. Adv. Mar. Biol. 23, 163–299.

Lips, U., Lips, I., Liblik, T., Kikas, V., Altoja, K., Buhhalko, N., Rünk, N., 2011w. Vertical dynamics of summer phytoplankton in a stratified estuary (Gulf of Finland, Baltic Sea). Ocean. Dyn. 61, 903–915. http://dx.doi.org/10.1007/s10236-011-0421-8.

Lund-Hansen, L.C., 2011. Subsurface chlorophyll maximum (SCM) location and extension in the water column as governed by a density interface in the strongly stratified Kattegat estuary. Hydrobiologia 673, 105–118. http://dx.doi.org/10.1007/s10750-011-0761-x.

Lund-Hansen, L.C., Vang, T., 2004. An inflow and intrusion event in the Little Belt at the North Sea–Baltic Sea transition and a related sub-surface bloom of Pseudo-nitzschia pseudodelicatissima. Estuar. Coast. Shelf Sci. 59, 265–276. http://dx.doi.org/10.1016/j.ecss.2003.09.004.

Mann, K.H., 2000. Ecology of Coastal Waters: With Implications For Management, 2nd ed. Wiley-Blackwell.

Martínez, A., Ortega, L., 2007. Seasonal trends in phytoplankton biomass over the Uruguayan Shelf. Cont. Shelf Res. 27, 1747–1758. http://dx.doi.org/10.1016/j.csr.2007.02.006.

O'Boyle, S., Silke, J., 2009. A review of phytoplankton ecology in estuarine and coastal waters around Ireland. J. Plankton Res. 32, 99–118. http://dx.doi.org/10.1093/plankt/fbp097.

Pedersen, F., 1994. The oceanographic and biological tidal cycle succession in shallow sea fronts in the North Sea and the English Channel. Estuar. Coast. Shelf Sci. 38, 249–269.

Redfield, A., Ketchum, B., Richards, F., 1963. The influence of organisms on the composition of sea-water. In: Hill, M. (Ed.), The Sea. Wiley, New York, pp. 26–77.

Sarker, J., Yamamoto, T., Hashimoto, T., 2009. Contribution of benthic microalgae to

the whole water algal biomass and primary production in Suo Nada, the Seto Inland Sea, Japan. J. Ocean. 65, 311–323.
Simpson, J.H., Hunter, J.R., 1974. Fronts in the Irish Sea. Nature 250, 404–406. http://dx.doi.org/10.1038/250404a0.
Strickland, J.D., Parsons, T., 1972. Practical Handbook of Seawater Analysis, Fisheries Research Board Bulletin. Fisheries Research Board of Canada, Ottawa.
Tada, K., Monaka, K., Morishita, M., Hashimoto, T., 1998. Standing stocks and production rates of phytoplankton and abundance of bacteria in the Seto Inland Sea, Japan. J. Ocean. 54, 285–295.
Takeoka, H., 2002. Progress in Seto Inland Sea Research. J. Ocean. 58, 93–107.
Takeoka, H., Matsuda, O., Yamamoto, T., 1993. Processes causing the chlorophyll *a* maximum in the tidal front in Iyo-Nada Japan. J. Ocean. 49, 57–70.
Takeoka, H., Ochi, T., Takatani, K., 1986. The anoxic water mass in Hiuchi-Nada Part 2. The Heat and Oxygen Budget Model. J. Ocean. Soc. Jpn. 42, 12–21.
Townsend, D.W., Thomas, M., 2002. Springtime nutrient and phytoplankton dynamics on Georges Bank. Mar. Ecol. Prog. Ser. 228, 57–74. http://dx.doi.org/10.3354/meps228057.
Welschmeyer, N.A., 1994. Fluorometric analysis of chlorophyll a in the presence of chlorophyll b and pheopigments. Limnol. Ocean. 39, 1985–1992.
Yamamoto, T., Hashimoto, T., Takeoka, H., Sugiyama, T., Matsuda, O., 2000. Middle layer intrusion as an important factor supporting phytoplankton productivity at a tidal front in Iyo Nada, the Seto Inland Sea, Japan. J. Ocean. 56, 131–139.
Yanagi, T., Koike, T., 1987. Seasonal variation in thermohaline and tidal fronts, Seto Inland Sea, Japan. Cont. Shelf Res. 7, 149–160.
Yanagi, T., Tamaru, H., 1990. Temporal and spatial variations in a tidal front. Cont. Shelf Res. 10, 615–627.
Yu, X., Guo, X., Takeoka, H. Fortnightly variations of tidal fronts, bottom thermal front and associated circulation in a semi-enclosed sea, J. Phys. Oceanogr. doi:10.1175/JPO-D-15-0071.1, in press.